Journal of Neurolinguistics 52 (2019) 100855

Contents lists available at ScienceDirect

Journal of Neurolinguistics

journal homepage: www.elsevier.com/locate/jneuroling

Research paper

Semantic unification modulates N400 and BOLD signal change in the brain: A simultaneous EEG-fMRI study

Zude Zhu[a,b,c,*], Marcel Bastiaansen[b,d,e], Jonathan G. Hakun[f], Karl Magnus Petersson[b,d], Suiping Wang[c,**], Peter Hagoort[b,d]

[a] School of Linguistic Sciences and Arts, Collaborative Innovation Center for Language Ability, Jiangsu Normal University, Xuzhou, China
[b] Donders Institute for Brain, Cognition and Behaviour, Radboud University, Nijmegen, the Netherlands
[c] School of Psychology, South China Normal University, Guangzhou, China
[d] Max Planck Institute for Psycholinguistics, Nijmegen, the Netherlands
[e] Academy for Leisure, NHTV Breda University of Applied Sciences, Breda, the Netherlands
[f] Department of Psychology, The Pennsylvania State University, State College, PA, USA

ARTICLE INFO

Keywords:
N400
EEG-fMRI
IFG
Semantic unification

ABSTRACT

Semantic unification during sentence comprehension has been associated with amplitude change of the N400 in event-related potential (ERP) studies, and activation in the left inferior frontal gyrus (IFG) in functional magnetic resonance imaging (fMRI) studies. However, the specificity of this activation to semantic unification remains unknown. To more closely examine the brain processes involved in semantic unification, we employed simultaneous EEG-fMRI to time-lock the semantic unification related N400 change, and integrated trial-by-trial variation in both N400 and BOLD change beyond the condition-level BOLD change difference measured in traditional fMRI analyses. Participants read sentences in which semantic unification load was parametrically manipulated by varying cloze probability. Separately, ERP and fMRI results replicated previous findings, in that semantic unification load parametrically modulated the amplitude of N400 and cortical activation. Integrated EEG-fMRI analyses revealed a different pattern in which functional activity in the left IFG and bilateral supramarginal gyrus (SMG) was associated with N400 amplitude, with the left IFG activation and bilateral SMG activation being selective to the condition-level and trial-level of semantic unification load, respectively. By employing the EEG-fMRI integrated analyses, this study among the first sheds light on how to integrate trial-level variation in language comprehension.

1. Introduction

Semantic unification is one of the core components of language comprehension (Hagoort, 2013; Hagoort, Baggio, & Willems, 2009; McCarthy, Nobre, Bentin, & Spencer, 1995). It refers to the process by which we construct complex meaning based on elementary lexical-semantic building blocks (i.e., words; cf. Hagoort, 2005). Semantic unification can be captured by manipulating the unification difficulty level during sentence comprehension. For instance, a given context may be associated with a highly expected upcoming word. If an unexpected word is presented, unification becomes more difficult than when an expected word is presented (Hagoort & Brown, 1994). High temporal resolution techniques such as event-related potentials (ERP; for review, see Hagoort, 2008)

* Corresponding author. School of Linguistic Sciences and Arts, Jiangsu Normal University, Xuzhou, 221009, China.
** Corresponding author. School of Psychology, South China Normal University, Guangzhou, 510631, China.
E-mail addresses: zhuzude@163.com (Z. Zhu), wangsuiping@m.scnu.edu.cn (S. Wang).

https://doi.org/10.1016/j.jneuroling.2019.100855
Received 3 November 2018; Received in revised form 27 June 2019; Accepted 28 June 2019
Available online 01 July 2019
0911-6044/

and magnetoencephalography (MEG; for review, see Salmelin, 2007) have found that the semantic unification load reaches its peak at around 400 ms after stimulus presentation (Kutas & Federmeier, 2011; Kutas & Hillyard, 1980), a component called as N400 and N400m in the ERP and the MEG studies, respectively.

Given its high spatial resolution, fMRI has been widely used to identify brain regions associated with semantic unification in vivo. Recent meta-analyses have revealed that unification is associated with activation across frontal-temporal-parietal regions (Hagoort et al., 2009; Hagoort & Indefrey, 2014; Lau, Phillips, & Poeppel, 2008; Vigneau et al., 2006), with highly consistent evidence of activation in the left inferior frontal gyrus (IFG, Hagoort et al., 2009), and sometimes with the temporal gyrus (Van Petten & Luka, 2006; Vandenberghe, Nobre, & Price, 2002).

Currently, the specificity of the left IFG activation to semantic unification remains unclear due to the number of potential cognitive processes involved in comprehension tasks. Specifically, the paradigms/tasks used in sentence fMRI studies may engage several cognitive processes beyond semantic unification (Zhu et al., 2012), such as conflict monitoring (van de Meerendonk, Indefrey, Chwilla, & Kolk, 2011), violation detection and repair (Kaan & Swaab, 2003), general cognitive control (Crinion, Lambon-Ralph, Warburton, Howard, & Wise, 2003) and task-specific strategies (Caplan, Chen, & Waters, 2008) such as working memory maintenance (Newman, Lee, & Ratliff, 2009).

Each of these confounding effects may recruit additional brain regions that mix with semantic unification related regions. Importantly, many of the cognitive processes conflated with semantic unification emerge at later time windows. For example, conflict monitoring (van de Meerendonk et al., 2011) and violation detection and repair (Kaan & Swaab, 2003) modulate the amplitude of a late positive component (LPC, around the 600–900 ms time window), which typically follows the N400 and thus can be easily separated from the N400 effect in ERP/MEG studies. However, because fMRI has poor temporal resolution, using this method alone makes it difficult to link brain activation specifically with semantic unification, as semantic unification and confounding effects like monitoring cannot easily be dissociated.

Simultaneously recording EEG and fMRI may be an effective means to parse brain signals by using variability in N400 amplitude to predict the fMRI signal (Laufs, Daunizeau, Carmichael, & Kleinschmidt, 2008; Lei, Qiu, Xu, & Yao, 2010). An advantage of this cross-methodological approach is that one could use trial-by-trial N400 amplitude to predict trial-by-trial BOLD signal change, constructing a direct association between modalities.

This methodology, while rarely used in the study of language, has been successfully employed to investigate the neural circuitry underlying ERP components (Debener et al., 2005; Eichele et al., 2005; Esposito, Mulert, & Goebel, 2009; Li, Mayhew, & Kourtzi, 2012; Morgan et al., 2010). For instance, Debener et al. (2005) used the amplitude of single-trial ERPs as a regressor in fMRI data analysis to isolate the cortical associates of the error-related negativity (ERN). They found that the ERN amplitude was correlated with BOLD changes in the rostral cingulate cortex, a region thought to play a key role in processing errors. Such evidence demonstrates the value of predicting hemodynamic responses with single-trial ERPs to yield a highly spatially resolved view of the sources of the ERP component in question, with the temporal resolution provided by electrophysiology.

There have been attempts to link N400 with BOLD activation using separate (Matsumoto, Iidaka, Haneda, Okada, & Sadato, 2005) and simultaneous (Geukes et al., 2013) recording in a semantic priming paradigm. In a semantic priming study (Matsumoto et al., 2005) with separated ERP and fMRI data collection, semantic retrieval-related N400 amplitude and brain activation in the left IFG, anterior cingulate cortex (ACC) and superior temporal gyrus (STG) were reduced in the related condition relative to the unrelated condition. Correlation analysis further suggested that the N400 amplitude change was linked with BOLD activation in the left STG, and this pattern was attributed to the modulation of access to the phonological representation caused by semantic priming.

By employing semantic priming manipulation and simultaneous EEG-fMRI recording, a second study (Geukes et al., 2013) found a significant N400 effect but no BOLD activation related to the semantic priming effect. The inconsistency between these studies, with the former finding widespread BOLD activation in frontal-temporal regions and the latter finding no BOLD differences between the primed condition and unprimed condition, may be due to the use of correlation analysis, which is unlike the trial-by-trial integration approach that maximizes the EEG-fMRI coupling.

Furthermore, the trial-by-trial integration approach can be used to distinguish condition-level and trial-level variation. In most traditional fMRI analyses, trials in the same condition were treated as the same in terms of intensity in estimating the BOLD response. Unlike stimuli in visual cognition studies, language stimuli always include trial-level variation. For instance, the semantic unification difficulty, which can be measured at the critical word window, is influenced by both the sentence context constraint and the cloze probability of the critical word, with semantic unification load varied at both conditional-level and trial-level. The N400 amplitude on the critical word could well capture both condition-level and trial-level variation, helping to better estimate language stimuli in an integrated EEG-fMRI analyses.

In the present study, we employed simultaneous EEG-fMRI to investigate the neural basis of semantic unification. Our primary aim was to establish whether a common unification-based signal is shared between N400 amplitude and BOLD signal change in the cortex. In the integrated EEG-fMRI analyses, we compared two models. One model (N400 model) only included an N400 regressor, based on single-trial estimates of the N400 amplitude in a 300–500 ms time window relative to onset of the critical word. We expected that regions contributing to semantic unification should reliably scale in activation magnitude with N400 modulations. Moreover, given that variability exists in semantic unification beyond condition effects (e.g., semantic unification differences between trials within each condition), we constructed a second model which included additional regressors corresponding to the experimental conditions (CONDITION + N400 model). In the CONDITION + N400 model, the condition-based task regressors were included to capture all of the BOLD variance associated with the experimental manipulation as per the usual conventions of fMRI analysis. However, in this second model, we expected to identify sources of N400 fluctuations that vary at the trial-to-trial level.

Table 1
Example of stimuli.

Conditions	Sentences	Cloze probability	Semantic acceptability
High cloze (HC)	Dutch: Die ziekte kan met het nieuwe **medicijn** veel beter behandeld worden. *English: That illness can be treated with the new **medicine** much better.*	0.68	6.27
Low cloze (LC)	Dutch: Die ziekte kan met het nieuwe **apparaat** veel beter behandeld worden. *English: That illness can be treated with the new **device** much better.*	0	5.35
Violation (SV)	Dutch: Die ziekte kan met het nieuwe **tijdstip** veel beter behandeld worden. *English: That illness can be treated with the new **moment** much better.*	0	1.77

Note. Critical words are presented in bold.

2. Methods

2.1. Participants

Twenty-eight healthy native speakers of Dutch participated in the experiment. All participants were right-handed, with normal or corrected-to-normal vision, and without neurological impairment. Four participants were excluded from further analysis, one because of technical problems (felt heat on electrodes during scanning) and three others because of excessive head motion in the scanner. Thus the final sample consisted of 6 males and 18 females (18–33 years of age, mean age of 23 years). All participants signed the written informed consent form according to the local ethics committee. Participants received either financial compensation or credit toward course requirements.

2.2. Stimulus materials

2.2.1. Experimental items

To manipulate the semantic unification load, we constructed three types of sentences: high cloze (HC), low cloze (LC) and semantic violation sentences (SV). First, sentences with a highly constraining context were constructed (HC condition). Each of these sentences was modified by replacing a semantically expected noun with a semantically unexpected noun that was nevertheless semantically congruent with the context (LC condition). Next the same semantically expected noun was replaced with a noun that was anomalous in the semantic sentence context (SV condition). The critical words (CWs) across conditions were matched in terms of word length (HC = 6.27, LC = 6.31, SV = 6.32, $F_{(2,\ 646)} = 3.42$, $p = 0.08$) and frequency (log frequency: HC = 2.71, LC = 2.70, SV = 2.69, $F_{(2,\ 646)} = 2.35$, $p = 0.10$). Frequency information was retrieved from WebCelex (http://celex.mpi.nl/), a database overseen by the Max Planck Institute for Psycholinguistics. See example sentences in Table 1.

2.2.2. Pre-tests

In order to validate our stimulus materials, we conducted a cloze probability test (with 20 participants who did not participate in the main experiment) and a semantic acceptability rating (with another 20 participants). We wanted CWs in the HC and LC conditions to be semantically acceptable, with high cloze and low cloze probability respectively. CWs in the SV condition were chosen because they had low cloze probability and were semantically anomalous.

The CW cloze probabilities were obtained by presenting sentences up until the word before the CW position. Participants were instructed to fill in the first noun that came to their mind and that made the sentence meaningful. The average cloze probability in the HC condition was 68% (SD = 19.5, ranging from 33.3% to 100%, with probabilities lower than 33.3% removed); the cloze probabilities in the other conditions were zero.

The sentences' semantic acceptability was measured using a 7-point Likert scale (1 = entirely unacceptable; 7 = fully acceptable). The average ratings for the HC, LC and SV conditions were 6.16 (SD = 0.63), 5.40 (SD = 1.02) and 1.77 (SD = 0.63), respectively. The acceptability ratings were significantly different across sentence types ($F_{(2,\ 646)} = 2952$, $p < .001$). The mean rating of the HC was higher than that of the LC ($p < .001$) and SV ($p < .001$), and the mean rating of the LC was higher than that of the SV ($p < .001$). The final experimental item set on which the cloze scores and semantic acceptability ratings were based consisted of 324 sets of sentences.

2.2.3. Filler items

For purposes of the experiment (see *Experimental lists* section) the CWs in the experimental item set appeared either at the 6th (50%) or the 7th (50%) position in each sentence. In order that the participants not expect the critical word in a specific position, 90 incongruent filler sentences were constructed, in which the violating words appeared at the 8th, 9th or 10th position in the sentence (30 sentences for each CW position). Further, to counterbalance the number of congruent and incongruent sentences, 90 filler items that were correct and semantically fully congruent were also constructed.

2.2.4. Experimental lists

The experiment consisted of two sessions, one session in which only EEG was recorded (in a standard EEG lab), and another session in which EEG and fMRI were recorded simultaneously. In this way, the EEG-alone recordings would provide a "gold standard"

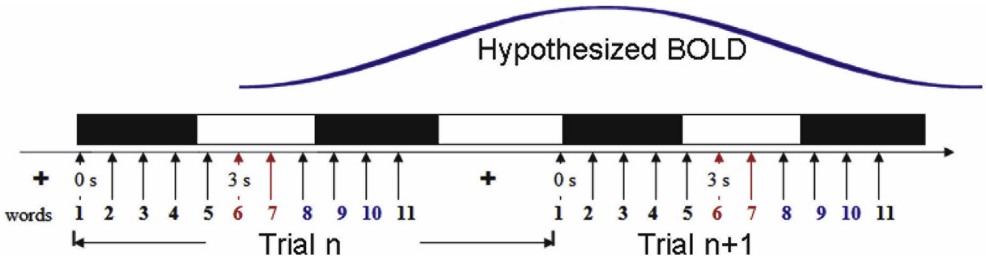

Fig. 1. Experimental design. Sentences were presented word by word. Critical words for experimental conditions occurred in 6th or 7th position (shown in red). During each TR, half the time was used for scanning (black rectangles), and other half was a silent period (white rectangles). The critical words were always presented during silent periods. Note that the peak of the BOLD response elicited by the critical word was sampled roughly at its maximum in the subsequent TR. (For interpretation of the references to colour in this figure legend, the reader is referred to the Web version of this article.)

for the EEG recordings in the scanner. Therefore the total item set of 504 sentences (324 experimental triplets sets, 180 fillers) was split into two halves. In each half, the 162 sentence sets were used to construct three lists via counterbalance procedure, each contained 54 high cloze, 54 low cloze, and 54 anomalous sentences. Additionally, 45 filler sentences with the violating word at the 8th, 9th or 10th position, and another 45 congruent filler sentences, were included. In total, each half thus included 252 sentences. Each participant was randomly assigned one of the lists for each session, with no sentence being read twice.

2.3. Procedure

The set-up was similar in the outside and inside scanner sessions, except that outside scanner the participants sat on a chair while inside scanner they lied on the bed and watched the screen on the top of the coil. In each session, participants were asked to read 252 sentences (162 of which were critical for the current study) for comprehension, which can capture the unification effect and reduce possible artifact due to make a response (Zhu et al., 2012). The sentences were presented in pseudorandom order in a word-by-word manner (Presentation software, Neurobehavioral Systems). The words were presented in white on a black background at the center of a computer screen, positioned approximately 80 cm away from the participant and approximately within 2.5° visual angle.

An important issue for simultaneous EEG-fMRI recording is to reduce noise. Sources of noise include gradient artifact and radio frequency pulse related artifact in the MRI scanner, which significantly confound the EEG signal. Moreover, heart beat related blood flow also induces vibration, which can cause a strong magnetic field and greatly increase the voltage. In either case, the artifact far exceeds the voltage change in brain activity (Allen, Polizzi, Krakow, Fish, & Lemieux, 1998).

To avoid these noises as much as possible, the present study adopted the sparse scanning design (Fig. 1). Specifically, at the beginning of each run, the participant saw a fixation cross, whose presentation was ended by the scanning. Then the sentences were presented word by word, with 300 ms for word presentation and 300 ms of blank screen after each word. Between trials was a fixation cross with duration of either 1650, 2400 or 3150 ms duration (2400 ms on average). A trial thus took 9 s on average. In such a design, the critical words for experimental conditions, which occurred in the 6th or 7th position, would be presented in the silent period (white blocks in the Fig. 1), to reduce the scanning related noise as much as possible.

Participants were told not to move or blink when individual words appeared. The 252 sentences were presented in 6 blocks of 42 trials each in a single run. The participants were asked to take a self-paced rest between blocks, lasting maximally 1 min. They had to press a button if they wanted to continue before the 1-min rest was over. All participants started with an EEG-only recording session. A minimum of two days later the EEG-fMRI recording session was conducted. The EEG outside scanner session lasted about 40 min, and the EEG-fMRI session lasted about 60 min.

2.4. EEG data acquisition

EEG data outside the scanner were collected from 29 standard channels (10/20 system, Fp1, Fp2, F3, F4, C3, C4, P3, P4, O1, O2, F7, F8, T7, T8, P7, P8, Fz, Cz, Pz, FC1, FC2, CP1, CP2, FC5, FC6, CP5, CP6, TP9 and TP10) by an actiCap (Brain products, Munich, Germany). Acticap is a relatively new type of cap that uses Ag/AgCl sensors with impedance conversion at the electrode level, leading to much lower noise compared to conventional passive electrodes. It also has three electrodes for eye movement measurement. The EEG data were referenced to the left mastoid during recording. The EEG recording was made continuously with a 10 s time constant and a 125 Hz low-pass filter, and was sampled at 500 Hz. All electrode impedances were kept below 10 kΩ.

2.5. EEG-fMRI data acquisition

2.5.1. EEG data acquisition

EEG in the MR environment was recorded with a MR-compatible cap (Easycap, Munich, Germany) equipped with 29 standard carbon wired Ag/AgCl electrodes (Fp1, Fp2, F3, F4, C3, C4, P3, P4, O1, O2, F7, F8, T7, T8, P7, P8, Fz, Cz, Pz, FC1, FC2, CP1, CP2, FC5, FC6, CP5, CP6, TP9 and TP10). Two additional bipolar electrode pairs were included. One pair was for the vertical

electrooculogram (EOG), with one electrode placed above the left eye and another electrode placed below the left eye. Another pair was for electrocardiograms, with one electrode placed in the clavicule, and the other one on the forearm. The EEG data were referenced to the FCz during recording. A 250-Hz analog hardware filter was placed between the electrode cap and the EEG amplifier (Brainproducts, Munich, Germany). The EEG was recorded with a 10 s time constant and a 100 Hz low-pass filter, and continuously sampled at 5 kHz in order to reduce MRI scanning related artifacts in off-line analysis. All electrode impedances were kept below 5 kΩ.

2.5.2. fMRI data acquisition

Data acquisition was performed using a Siemens Trio 3T MR. Whole-brain echo-planar images (EPIs) were acquired in interleaved scanning with ascending slice order (TR = 4500 ms, silent period = 2250 ms, TE = 30 ms, flip angle = 80°, 33 slices, slice thickness = 3 mm, 0.5 mm gap between slices, voxel size 3.5 × 3.5 × 3.5 mm^3). We used interleaved scanning in order to ensure that the critical words in each sentence were presented during a silent period (see Fig. 1). This allowed us to record EEG data that was free of gradient artifacts. As illustrated in Fig. 1, we took advantage of BOLD's delayed timing, and made sure the peak of the BOLD signal elicited by critical words was adequately sampled. A high resolution T1 weighted scan was acquired for each participant after the functional runs using an MPRAGE sequence (192 slices, TE = 3.03 ms; voxel size 1 × 1 × 1 mm^3).

2.6. EEG data analysis

2.6.1. EEG outside the scanner

The EEG data were re-referenced off-line to the average of both mastoids, and then filtered with a 0.5–25 Hz bandpass filter. Critical epochs ranged from −200 ms to 1200 ms relative to the onset of the critical word, with −200 ms to 0 ms serving as the baseline. The artifact rejection criterion was ± 90 μV. Epochs that included eye blinks were removed by visual inspection. On average, the number of trials for HC, LC and SV after artifact rejection was 52, with no significant differences in trial numbers between the three conditions ($F < 1$). For each participant, the remaining trials were then averaged for each condition separately. For a statistical evaluation of the ERP data recorded in the outside-the-scanner session, subject-averaged N400 amplitudes were computed in a 300–500 ms post-CW interval. After that, the values of five electrodes were averaged in four regions: left anterior (Fp1, F3, F7, FC1 and FC5), left posterior (CP1, CP5, P3, P7 and O1), right anterior (Fp2, F4, F8, FC2 and FC6) and right posterior (CP2, CP6, P4, P8 and O2). Then, a three-way repeated measures ANOVA was performed on the averaged data, with the following within subject factors: Condition (HC, LC, SV), Hemisphere (Left, Right) and Region (Anterior, Posterior). When the degrees of freedom in the numerator was larger than 1, Greenhouse-Geisser correction was applied. Post-hoc contrasts were computed when effects involving Condition (the three-level factor) were significant.

2.6.2. EEG inside the scanner

The EEG data recorded inside the MR scanner were corrected for gradient and ballistocardiac artifacts along the lines described in previous studies (Allen et al., 1998; Allen, Josephs, & Turner, 2000) with Vision Analyzer (Brainproducts, Munich, Germany). The MR-denoised EEG data were low-pass filtered at 25 Hz, down-sampled to 250 Hz and re-referenced to the average of both mastoids. The original reference electrode was recalculated as FCz, yielding a total of 30 EEG channels. Because high noise naturally existed in the scanner, a 1–8 Hz bandpass filter was applied to the data (see similar parameter settings in Bénar et al., 2007). This frequency band appropriately captures the N400 frequency range and thus the filter should remove most of the noise but leave the N400 intact. Critical epochs ranged from −200 ms to 1200 ms relative to the onset of the critical word, with −200 ms to 0 ms serving as the baseline. A relatively liberal artifact rejection criterion was adopted (rejection trials with amplitudes exceeding ± 120 μV compared to baseline), in order to retain acceptable numbers of trials for the integrated EEG-fMRI data analysis. Epochs that included eye blinks were removed by visual inspection. The number of trials for the HC, LC and SV conditions after artifact rejection was 45, 44, and 45 respectively, with no significant difference in number of trials among conditions ($F < 1$). For each participant, the remaining trials were then averaged for each condition separately.

Next, to better capture the N400 component, the data from all three conditions were concatenated and subjected to an extended infomax Independent Component Analysis (ICA; Lee, Girolami, & Sejnowski, 1999) for each participant, with EEGLAB 6.0 (Delorme & Makeig, 2004). For each participant, one single independent component (IC) was selected on the basis of three criteria: (1) the IC had a maximum deflection from zero around 400 ms; (2) the IC had an N400 scalp distribution (i.e., a maximum at or around electrode position Pz); and (3) the time-locked averages per condition of this IC showed roughly the same N400 effects as in the EEG data recorded in the outside-the-scanner session for that participant.

For a statistical evaluation of the ERP data recorded in the inside-the-scanner session, subject-averaged N400 amplitudes were computed in a 300–500 ms post-CW interval. These values were subjected to a repeated measures ANOVA for data before and after ICA separately, with the same procedure used in the outside scanner session.

2.6.3. N400 regressor construction

For the integrated analysis of the simultaneously recorded EEG and fMRI data, we constructed participant-specific single-trial EEG regressors as follows. The time course of the selected IC was back-projected onto the scalp electrodes to recover polarity and amplitude scaling. Then for each trial the mean amplitude in a 300–500 ms window after CW onset was extracted from the time course at Pz. (Note that at this point all channels have the same time course, because only one IC was back-projected.) Values for trials that were rejected because of artifacts were then replaced by the average value for the corresponding condition. A z-transformation was

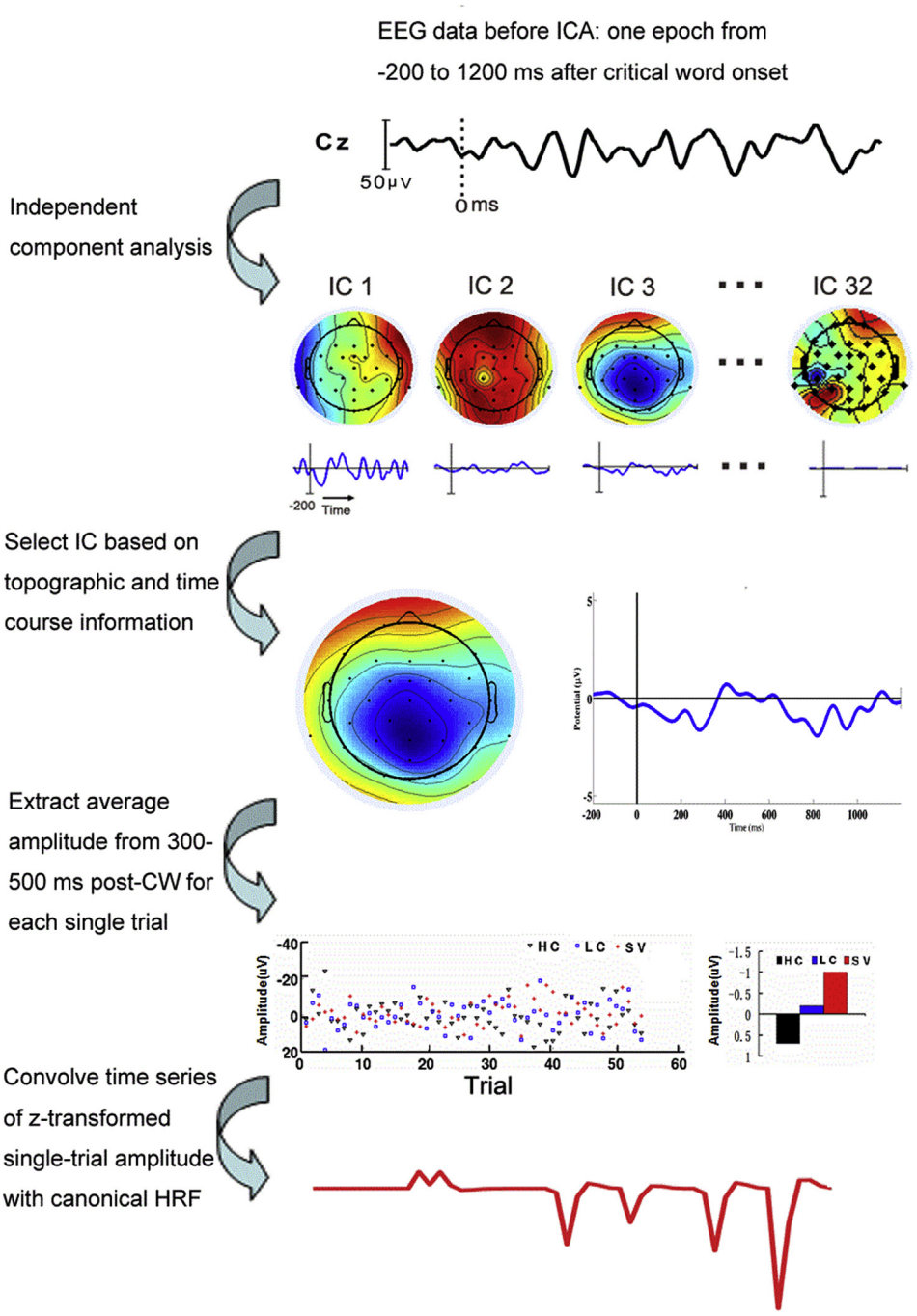

Fig. 2. Schematic of data analysis procedure for EEG regressor construction.

then applied to the resulting values. Outliers (defined as $|z| > 3$) were replaced by the average value for the corresponding condition, and another z-transformation was applied (< 1% of total number of trials). The resulting z-values were then inserted at the appropriate places in the regressor time course (see *Linear modeling* section), and the entire time course was convolved with the canonical haemodynamic response function (HRF) provided by SPM5 (www.fil.ion.ucl.ac.uk/spm). The entire data analysis and regressor construction procedure is illustrated in the flowchart in Fig. 2, using data from one participant as an illustration.

2.7. fMRI data analysis

2.7.1. Preprocessing

Data were analyzed with SPM5 (www.fil.ion.ucl.ac.uk/spm). Preprocessing included motion correction by means of rigid body registration along three rotations and three translations, correction of slice acquisition time, co-registration between EPI and structural images, normalization to a standard MNI T1 template and interpolation to a voxel size of $2 \times 2 \times 2\,mm^3$, then high-pass filtering (cut-off cycle = 128 s) and spatial filtering with an isotropic Gaussian kernel (FWHM = 8 mm). The statistical analysis was performed within the general linear model framework first at the single-subject level, and second at the random effects group level.

2.7.2. Linear modeling

Parametric modulation of BOLD responses was estimated by combining the three experimental conditions into one regressor (HC, LC and SV were represented by −1 0 1, respectively), as done in a previous study (Zhu et al., 2012). Using this regressor, the CW onset was the event onset and the event duration was set at 600 ms (the stimulus onset asynchrony in the experiment). The filler regressors consisted of all the non-critical words, the filler sentences, and the self-paced break period. The parametric modulation regressor, the filler regressors and the motion parameters were all included in a linear model.

2.7.3. Integrated EEG-fMRI analyses

For the integrated EEG-fMRI analyses we designed two standard general linear models. The first (N400 model) included the N400 regressor (along with regressors for the filler trials and the motion parameters), based on single-trial estimates of the N400 amplitude in a 300–500 ms post-CW time window. The second model (CONDITION + N400 model) was identical to the first but included three additional regressors corresponding to the three experimental conditions.

In the N400 model, the only regressor that models the experimental manipulation is the N400 regressor. We therefore expected the N400 regressor to capture all BOLD signal variance that is in any way related to changes in semantic unification load. This should hold for all types of BOLD changes, including both condition-level and trial-level effects.

In contrast, in the CONDITION + N400 model, the task regressors will capture all BOLD signal variance associated with the experimental manipulation of cloze probability, while the remaining residual variance in the N400 regressor will capture only the BOLD signal changes above and beyond those captured by the task regressors. To examine the influence of condition versus trial-by-trial modulation, the present study compared the BOLD correlation with the N400 regressor in the N400 model (sensitive to both condition-level and trial-level N400 fluctuation) and the BOLD correlation with the N400 regressor in the CONDITION + N400 model (sensitive to trial-level N400 fluctuation).

2.8. Statistical analyses

The fMRI data were analyzed statistically using the general linear model framework and statistical parametric mapping in a two-step mixed-effects summary-statistics procedure (Friston, Ashburner, Kiebel, Nichols, & Penny, 2007). For the parametric modulation analysis, the parametric modulation coefficient from the first level analysis was used as input for the second level analysis (one sample *t*-test). For the N400 model and the CONDITION + N400 model, the N400 regressor coefficient from the first-level analysis was used as input for the one-sample *t*-test at the second level, in order to test for any correlation between N400 and BOLD.

Monte Carlo simulations for this contrast were conducted using the AlphaSim program (http://afni.nimh.nih.gov/pub/dist/doc/manual/AlphaSim.pdf; Cox, Chen, Glen, Reynolds, & Taylor, 2017) to determine the appropriate combination of significance level and cluster threshold required to reach a corrected significance level of $p < .05$, taking into account both native space voxel dimensions and the effective smoothness of our preprocessed data. The Monte Carlo simulations used 10,000 iterations and indicated an uncorrected significance level of $p < .001$ and cluster threshold of 65 voxels in order to reach a corrected significance level of $p < .05$. Using this threshold, however, we did not observe significant clusters in the integrated EEG-fMRI analyses. To explore the potential correspondence between EEG and fMRI, we then used a more liberal threshold for uncorrected significance of $p < .01$ and a cluster threshold of 220 voxels in order to reach a corrected significance level of $p < .05$. All local maxima are reported as MNI coordinates. Relevant anatomical landmarks were identified and Brodmann areas were defined using the Talairach atlas (Talairach & Tournoux, 1988).

3. Results

3.1. ERP data

Grand average ERPs for the three conditions (HC, LC and SV) were computed (1) for the outside-the-scanner session (EEG alone); (2) for the inside-the-scanner session (EEG-fMRI) before ICA; and (3) after ICA. See Fig. 3.

For the data in the outside-the-scanner session (Fig. 3A), statistical analysis revealed a main effect of Hemisphere ($F_{(1, 23)} = 14.49$, $p = .001$; larger negativity in the right hemisphere) and Condition ($F_{(2, 46)} = 43.74$, $p < .001$). Post-hoc comparisons for the main effect of Condition revealed that LC was more negative than HC ($p < .001$), SV was more negative than HC ($p < .001$), and SV was more negative than LC ($p < .001$), showing that semantic unification load parametrically modulated N400 amplitude. There were no significant interaction effects (all p values $> .15$).

For the EEG data in the inside-the-scanner session before ICA (Fig. 3B), the only significant effect was a main effect of Hemisphere

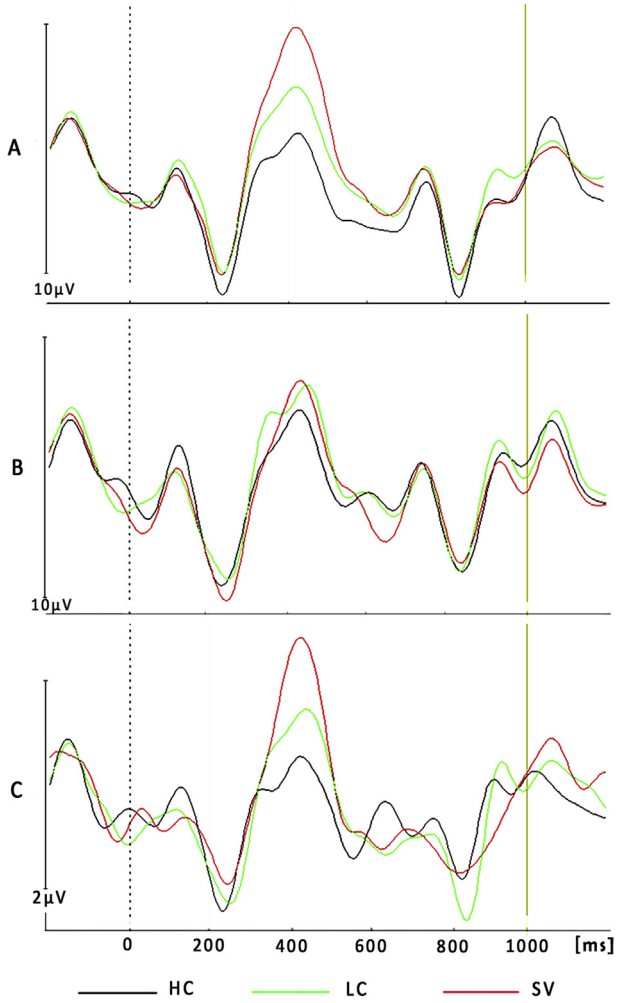

Fig. 3. Grand average ERPs at Cz, for each of the three conditions. (A) ERPs for EEG data recorded outside the scanner, (B) ERPs for inside scanner data, before ICA, and (C) ERPs for inside scanner data, after ICA.

($F_{(1, 23)} = 7.11$, $p = .014$), indicating that N400 amplitudes were more negative in the left than in the right hemisphere. There were no effects that included Condition. For the data in the inside-the-scanner session after ICA (Fig. 3C), statistical analysis revealed a main effect of Condition ($F_{(2, 46)} = 14.92$, $p < .001$), which confirmed the IC selection results (see *EEG inside the scanner* section). In addition, there was a significant interaction between Condition and Region ($F_{(2, 46)} = 3.88$, $p = .028$). Follow-up contrasts revealed a parametric N400 modulation (i.e., HC < LC < SV in terms of absolute magnitude), for both anterior (p values < .02) and posterior (p values < .025) regions.

3.2. fMRI data

For the conventional fMRI analyses, we examined the parametric modulation of BOLD by unification load. The positive parametric modulation showed activation in both left and right IFG, in left superior/middle temporal gyrus (S/MTG) and ACC (see Fig. 4), with the highest signals in SV and lowest signals in HC. All activated regions are listed in Table 2.

3.3. Integrated EEG and fMRI analyses

Table 3 presents the significant effect in the integrated EEG-fMRI analyses. In the N400 model, the N400 regressor showed a significant negative correlation with activation in the left IFG, bilateral supramarginal gyrus (SMG) (Fig. 5A). In the CONDITION +N400 model, activations negatively correlated with the N400 regressor were obtained in the bilateral SMG only (Fig. 5B).

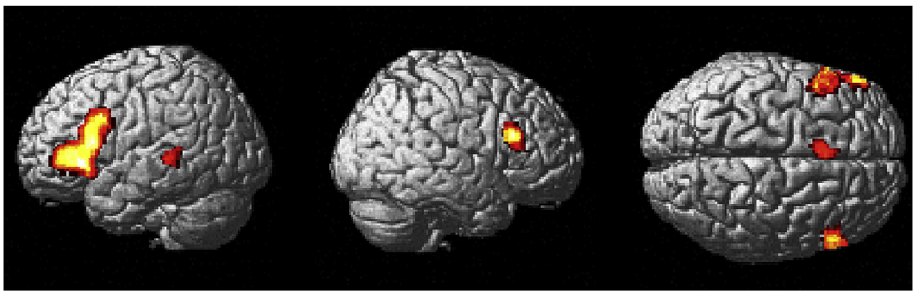

Fig. 4. Significant parametric modulation (PM) in a conventional GLM.

Table 2
Parametric modulation of semantic unification.

Regions	Hem	BA	Voxels	Z-score	X	Y	Z
Inferior Frontal Gyrus	left	9/44/45	2441	4.72	−48	12	30
Inferior Frontal Gyrus	right	9	477	4.24	54	22	26
Anterior Cingulate Cortex	left	6	200	4.21	−4	18	52
Superior/Middle Temporal Gyrus	left	22	166	3.81	−50	−36	4

Note: Hem, hemisphere. BA, Brodmann's area. X, Y, and Z presented the stereotaxic coordinates according to Montreal Neurological Institute (MNI) template.

Table 3
N400-BOLD correlations.

Regions	Hem	BA	Voxels	Z-score	X	Y	Z
N400 model							
Middle/inferior Frontal Gyrus	left	9/45	378	3.16	−44	30	38
Supramaginal Gyrus	left	40	506	2.91	−40	−52	46
Supramaginal Gyrus	right	40	435	3.17	58	−50	40
Condition + N400 model							
Supramaginal Gyrus	left	40	453	3.03	−40	−52	42
Supramaginal Gyrus	right	40	766	3.29	58	−50	40

Note: Hem, hemisphere. BA, Brodmann's area. X, Y, and Z presented the stereotaxic coordinates according to Montreal Neurological Institute (MNI) template.

4. Discussion

The aim of this study was to investigate the neural basis of semantic unification. In replication of previous findings we found that semantic unification load parametrically modulated both the N400 amplitude and the BOLD signal change in several brain regions. However, in line with our argument that experimental manipulations are insufficient to identify regions specific to semantic unification, integrated analyses of N400 amplitude and BOLD signal revealed a considerably reduced number of regions that tracked the semantic unification load. More importantly, integrated EEG-fMRI analyses further showed that BOLD signal change in the left IFG was central to differences in semantic unification load brought on by the manipulation of cloze probability. Trial-level fluctuations across all three conditions, on the other hand, appeared to map onto activity in the bilateral SMG. The details of these findings and their implications for understanding the neurobiology of semantic unification are discussed below.

In the present study, by showing parametric increase of N400 amplitude from HC to LC and SV we demonstrated that semantic unification load was successfully manipulated. These results are in line with previous studies that manipulated cloze probability (Hagoort & Brown, 1994; Kutas & Federmeier, 2011; Zhu et al., 2012). We also observed that semantic unification load parametrically modulated the BOLD signal change in the bilateral IFG and left MTG, regions that have previously been associated with semantic unification during sentence comprehension (Hagoort et al., 2009; Hagoort & Indefrey, 2014; Lau et al., 2008).

Here we argue that a significant modulation of the BOLD signal through experimental manipulation of unification load alone is not enough to conclude that a region is specified to unification, given the variety of additional processes that may be affected by the task (Lau et al., 2008; Van Petten & Luka, 2006; Vartiainen, Liljestrom, Koskinen, Renvall, & Salmelin, 2011). To this point, the results of our parametric fMRI analysis showed that a host of regions were activated by, and scaled in activation with, the manipulation of semantic unification load.

As a first means of limiting the influence of such confounding effects on our fMRI results, we explicitly tested the correspondence between N400 and the BOLD signal by using the N400 amplitude to predict BOLD signal changes. Compared with previous studies that found a weak association between N400 and BOLD activation (Geukes et al., 2013; Matsumoto et al., 2005), the current study

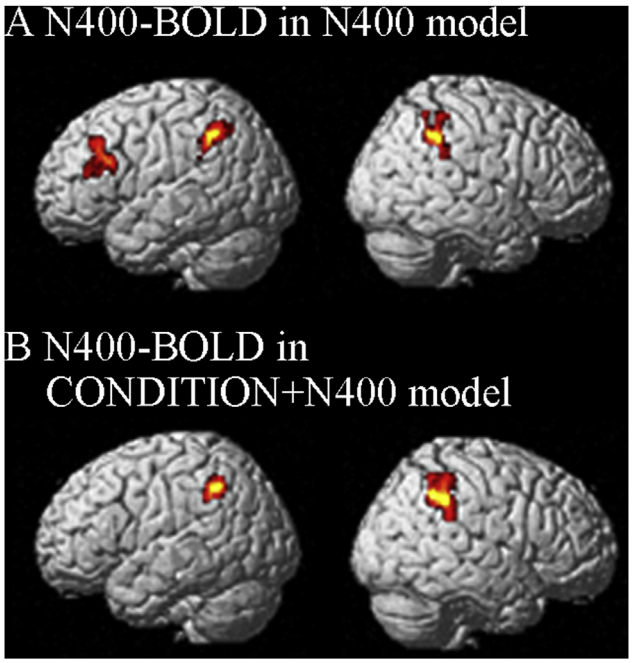

Fig. 5. N400 regressor related BOLD signal change. (A) Negative correlation between N400 and BOLD in the N400 model. (B) Negative correlation between N400 and BOLD in the CONDITION + N400 model.

showed a strong connection between N400 amplitude and BOLD amplitude in several regions, including the left IFG and bilateral SMG. The discrepancy between the present study and previous studies may be due to methodological differences across studies. Previous studies used a correlation approach at the subject level in a word level semantic priming paradigm. By contrast, the integrated EEG-fMRI analyses revealed a direct association between amplitude changes in the N400 time window and the BOLD signal changes in left IFG and bilateral SMG, in relation to semantic unification during sentence comprehension. These results are the first to reveal a direct correspondence between the N400 and BOLD signal in multiple brain regions with a trial-by-trial coupling approach.

A further critical analysis in the present study is the comparison of condition-level and trial-level N400-BOLD association. In fact, in the current study, semantic unification load varied across not only at condition-level but also at trial-level. While the main source of semantic unification load is the mapping difficulty between the critical word and the context across conditions, there was difference across sentences even within the same condition. However, parametric modulation in traditional analyses could only map to the condition variation, and the N400 model includes all variations at both the condition-level and trial-level. To dissociate condition-level and trial-level variation in the relationship between N400 amplitude and BOLD signal, we tested a second integrated EEG-fMRI model with the experimental conditions included. After the three condition regressors were added to this model, the N400-BOLD correlation was no longer present in the left IFG. The presence and absence of the left IFG activation in the N400 and CONDITION + N400 model, respectively, are crucial in our opinion. It revealed that the activation in the left IFG and bilateral SMG responds to condition-level and trial-level variation, respectively.

The correspondence of N400 amplitude and the left IFG activation found in the integrated EEG-fMRI analyses extends our recent findings on the semantic unification load modulations of N400 and left IFG activation in each modality separately (Hagoort, Hald, Bastiaansen, & Petersson, 2004; Zhu et al., 2012). Unlike the traditional analysis that commonly treats all trials in the same condition with the same intensity in modulating HRF, the success in isolating trial-level variation in the EEG-fMRI integrated analyses sheds light on language studies. As language stimuli cannot be kept the same in terms of attribution across trials in the same condition, trial-level fluctuation provides a window to reveal the underlying brain response during a language task.

The dissociated condition-level and trial-level effect of semantic unification fit well with a recent theory (Baggio & Hagoort, 2011) that the left IFG and temporoparietal regions constitute a processing cycle, with the temporal/parietal regions providing feed forward information to the left IFG, from where feedback is sent to these regions. This is consistent with previous work that showed a prediction effect in left PFC (Kerns, Cohen, Stenger, & Carter, 2004). The BOLD signal change in the left IFG is presumably a sustained state effect, which is less affected by trial-by-trial variation (Hagoort, 2013) and is thus consistent with our current results showing that condition unification load rather than single trial N400 variations contribute to the BOLD signal change in the left IFG.

Previous fMRI studies did not address the relationship between trial-level fluctuation of semantic unification and activation in the bilateral SMG. However, the association between language comprehension and activation of the SMG has been found in multiple studies (Dale et al., 2000; Dronkers, Wilkins, Van Valin, Redfern, & Jaeger, 2004; Guillem, Rougier, & Claverie, 1999; Tse et al., 2007). The SMG is also functionally (Xiang, Fonteijn, Norris, & Hagoort, 2010) and structurally (Catani & Jones, 2005) connected

with the left IFG.

Although the SMG is a region with multiple functions (Deschamps, Baum, & Gracco, 2013), there is clear evidence suggesting that the SMG contributes to verbal working memory. For instance, it was recently found that repetitive transcranial magnetic stimulation over the left SMG impairs verbal working memory performance in an n-back task (Deschamps et al., 2013). Given that associations between the N400 and verbal working memory have been found in previous studies (Gunter, Wagner, & Friederici, 2003; Salisbury, 2004), the correspondence of N400 trial variation and the bilateral SMG activation may reflect some effect of verbal working memory in our task.

It should be noted that we found N400-BOLD associations in the left IFG and bilateral SMG, but not in temporal regions. Temporal cortex is considered to be a strong neural generator of the N400 (Lau, Gramfort, Hamalainen, & Kuperberg, 2013; McCarthy et al., 1995), especially in MEG studies (Dale et al., 2000; Liljestrom, Hulten, Parkkonen, & Salmelin, 2009). While both EEG and MEG have high temporal resolution and have been widely used, the characteristics inherent to source localization within each modality may explain discrepancies identified in earlier research (e.g., sensitivity to tangential versus radially oriented dipoles and sensitivity to local field potentials; Logothetis, 2008). Future studies are needed to explore these discrepancies.

Moreover, activations in the right IFG and ACC were associated with semantic unification load but not the N400 amplitude. While these regions have been observed in semantic unification studies, they were linked with task difficulty (Zhu et al., 2009) and monitoring (Kerns et al., 2004; van de Meerendonk et al., 2011), not semantic unification per se. Monitoring or repairing during sentence comprehension was associated with the LPC, a component that occurred after the N400. The absence of these regions in the integrated EEG-fMRI analyses confirmed our expectation that trial-by-trial N400-BOLD integration analyses does not capture effects outside of N400 time window. The results further revealed the EEG-fMRI integrated analyses could be used to isolate time sensitive effects like semantic unification load. A limitation is that our integrated EEG-fMRI analyses were affected by the low signal-to-noise ratio due to the scanning related noise, thus a liberal threshold was adopted (Messina et al., 2018). Further studies might change the experimental design, stimuli and approach to analysis to clarify the results.

In conclusion, our results show that the left IFG and bilateral SMG play a central role in semantic unification. The integrated EEG-fMRI methodology that we have used represents a potentially powerful way to bridge the gap between the often disparate bodies of EEG and fMRI literature, and could additionally allow us to model trial-by-trial fluctuations in brain activity, thereby increasing the sensitivity of the analysis of brain activity recorded during experimental paradigms.

Acknowledgments

This research was supported by grants from the Natural Science Foundation of China (NSFC 31571136, 31100811 and 31871133), the National Social Science Foundation of China (15AZD048), and Priority Academic Program Development of Jiangsu Higher Education Institutions, Jiangsu. We thank Dr. Li Ma from Jiangsu Normal University for her assistance in proofreading.

References

Allen, P., Josephs, O., & Turner, R. (2000). A method for removing imaging artifact from continuous EEG recorded during functional MRI. *NeuroImage, 12*(2), 230–239.
Allen, P., Polizzi, G., Krakow, K., Fish, D., & Lemieux, L. (1998). Identification of EEG events in the MR scanner: The problem of pulse artifact and a method for its subtraction. *NeuroImage, 8*(3), 229–239.
Baggio, G., & Hagoort, P. (2011). The balance between memory and unification in semantics: A dynamic account of the N400. *Language & Cognitive Processes, 26*, 1338–1367.
Bénar, C., Schön, D., Grimault, S., Nazarian, B., Burle, B., Roth, M., et al. (2007). Single trial analysis of oddball event related potentials in simultaneous EEG fMRI. *Human Brain Mapping, 28*(7), 602–613.
Caplan, D., Chen, E., & Waters, G. (2008). Task-dependent and task-independent neurovascular responses to syntactic processing. *Cortex, 44*(3), 257–275.
Catani, M., & Jones, D. (2005). Perisylvian language networks of the human brain. *Annals of Neurology, 57*(1), 8–16.
Cox, R. W., Chen, G., Glen, D. R., Reynolds, R. C., & Taylor, P. A. (2017). fMRI clustering and false-positive rates. *Proceedings of the National Academy of Sciences of the United States of America, 114*(17), E3370–E3371.
Crinion, J. T., Lambon-Ralph, M. A., Warburton, E. A., Howard, D., & Wise, R. J. S. (2003). Temporal lobe regions engaged during normal speech comprehension. *Brain, 126*(5), 1193–1201.
Dale, A. M., Liu, A. K., Fischl, B. R., Buckner, R. L., Belliveau, J. W., Lewine, J. D., et al. (2000). Dynamic statistical parametric mapping: Combining fMRI and MEG for high-resolution imaging of cortical activity. *Neuron, 26*(1), 55–67.
Debener, S., Ullsperger, M., Siegel, M., Fiehler, K., Von Cramon, D., & Engel, A. (2005). Trial-by-trial coupling of concurrent electroencephalogram and functional magnetic resonance imaging identifies the dynamics of performance monitoring. *Journal of Neuroscience, 25*(50), 11730.
Delorme, A., & Makeig, S. (2004). EEGLAB: An open source toolbox for analysis of single-trial EEG dynamics including independent component analysis. *Journal of Neuroscience Methods, 134*(1), 9–21.
Deschamps, I., Baum, S. R., & Gracco, V. L. (2013). On the role of the supramarginal gyrus in phonological processing and verbal working memory: Evidence from rTMS studies. *Neuropsychologia, 53C*, 39–46.
Dronkers, N. F., Wilkins, D. P., Van Valin, R. D., Jr., Redfern, B. B., & Jaeger, J. J. (2004). Lesion analysis of the brain areas involved in language comprehension. *Cognition, 92*(1–2), 145–177.
Eichele, T., Specht, K., Moosmann, M., Jongsma, M., Quiroga, R., Nordby, H., et al. (2005). Assessing the spatiotemporal evolution of neuronal activation with single-trial event-related potentials and functional MRI. *Proceedings of the National Academy of Sciences of the United States of America, 102*(49), 17798.
Esposito, F., Mulert, C., & Goebel, R. (2009). Combined distributed source and single-trial EEG-fMRI modeling: Application to effortful decision making processes. *NeuroImage, 47*(1), 112–121.
Friston, K. J., Ashburner, J. T., Kiebel, S. J., Nichols, T. E., & Penny, W. D. (2007). *Statistical parametric mapping: The analysis of functional brain images.* San Diego, CA: Academic Press.
Geukes, S., Huster, R. J., Wollbrink, A., Junghofer, M., Zwitserlood, P., & Dobel, C. (2013). A large N400 but no BOLD effect: Comparing source activations of semantic priming in simultaneous EEG-fMRI. *PLoS One, 8*(12), e84029.
Guillem, F., Rougier, A., & Claverie, B. (1999). Short- and long-delay intracranial ERP repetition effects dissociate memory systems in the human brain. *Journal of Cognitive Neuroscience, 11*(4), 437–458.

Gunter, T. C., Wagner, S., & Friederici, A. D. (2003). Working memory and lexical ambiguity resolution as revealed by ERPs: A difficult case for activation theories. *Journal of Cognitive Neuroscience, 15*(5), 643–657.
Hagoort, P. (2005). On broca, brain, and binding: A new framework. *Trends in Cognitive Sciences, 9*(9), 416–423.
Hagoort, P. (2008). The fractionation of spoken language understanding by measuring electrical and magnetic brain signals. *Philosophical Transactions of the Royal Society B: Biological Sciences, 363*(1493), 1055–1069.
Hagoort, P. (2013). MUC (memory, unification, control) and beyond. *Frontiers in Psychology, 4*, 416.
Hagoort, P., Baggio, G., & Willems, R. M. (2009). Semantic unification. In M. S. Gazzaniga (Ed.). *The cognitive neurosciences* (pp. 819–836). London: MIT Press.
Hagoort, P., & Brown, C. (1994). Brain responses to lexical ambiguity resolution and parsing. In C.CJr., L. Frazier, & K. Rayner (Eds.). *Perspectives on sentence processing* (pp. 45–80). Hilsdale NY: Lawrence Erlbaum Associates.
Hagoort, P., Hald, L., Bastiaansen, M., & Petersson, K. M. (2004). Integration of word meaning and world knowledge in language comprehension. *Science, 304*(5669), 438–441.
Hagoort, P., & Indefrey, P. (2014). The neurobiology of language beyond single words. *Annual Review of Neuroscience, 37*, 347–362.
Kaan, E., & Swaab, T. Y. (2003). Repair, revision, and complexity in syntactic analysis: An electrophysiological differentiation. *Journal of Cognitive Neuroscience, 15*(1), 98–110.
Kerns, J. G., Cohen, J. D., Stenger, V. A., & Carter, C. S. (2004). Prefrontal cortex guides context-appropriate responding during language production. *Neuron, 43*(2), 283–291.
Kutas, M., & Federmeier, K. D. (2011). Thirty years and counting: Finding meaning in the N400 component of the event-related brain potential (ERP). *Annual Review of Psychology, 62*, 621–647.
Kutas, M., & Hillyard, S. A. (1980). Reading senseless sentences: Brain potentials reflect semantic incongruity. *Science, 207*(4427), 203–205.
Laufs, H., Daunizeau, J., Carmichael, D. W., & Kleinschmidt, A. (2008). Recent advances in recording electrophysiological data simultaneously with magnetic resonance imaging. *NeuroImage, 40*(2), 515–528.
Lau, E. F., Gramfort, A., Hamalainen, M. S., & Kuperberg, G. R. (2013). Automatic semantic facilitation in anterior temporal cortex revealed through multimodal neuroimaging. *Journal of Neuroscience, 33*(43), 17174–17181.
Lau, E. F., Phillips, C., & Poeppel, D. (2008). A cortical network for semantics: (de)constructing the N400. *Nature Reviews Neuroscience, 9*(12), 920–933.
Lee, T., Girolami, M., & Sejnowski, T. (1999). Independent component analysis using an extended infomax algorithm for mixed subgaussian and supergaussian sources. *Neural Computation, 11*(2), 417–441.
Lei, X., Qiu, C., Xu, P., & Yao, D. (2010). A parallel framework for simultaneous EEG/fMRI analysis: Methodology and simulation. *NeuroImage, 52*(3), 1123–1134.
Liljestrom, M., Hulten, A., Parkkonen, L., & Salmelin, R. (2009). Comparing MEG and fMRI views to naming actions and objects. *Human Brain Mapping, 30*(6), 1845–1856.
Li, S., Mayhew, S. D., & Kourtzi, Z. (2012). Learning shapes spatiotemporal brain patterns for flexible categorical decisions. *Cerebral Cortex, 22*(10), 2322–2335.
Logothetis, N. K. (2008). What we can do and what we cannot do with fMRI. *Nature, 453*(7197), 869–878.
Matsumoto, A., Iidaka, T., Haneda, K., Okada, T., & Sadato, N. (2005). Linking semantic priming effect in functional MRI and event-related potentials. *NeuroImage, 24*(3), 624–634.
McCarthy, G., Nobre, A. C., Bentin, S., & Spencer, D. D. (1995). Language-related field potentials in the anterior-medial temporal-lobe .1. Intracranial distribution and neural generators. *Journal of Neuroscience, 15*(2), 1080–1089.
van de Meerendonk, N., Indefrey, P., Chwilla, D. J., & Kolk, H. H. (2011). Monitoring in language perception: Electrophysiological and hemodynamic responses to spelling violations. *NeuroImage, 54*(3), 2350–2363.
Messina, R., Rocca, M. A., Colombo, B., Pagani, E., Falini, A., Goadsby, P. J., et al. (2018). Gray matter volume modifications in migraine: A cross-sectional and longitudinal study. *Neurology, 91*, e280–e292.
Morgan, H. M., Jackson, M. C., Klein, C., Mohr, H., Shapiro, K. L., & Linden, D. E. (2010). Neural signatures of stimulus features in visual working memory–a spatiotemporal approach. *Cerebral Cortex, 20*(1), 187–197.
Newman, S. D., Lee, D., & Ratliff, K. L. (2009). Off-line sentence processing: What is involved in answering a comprehension probe? *Human Brain Mapping, 30*(8), 2499–2511.
Salisbury, D. F. (2004). Semantic memory and verbal working memory correlates of N400 to subordinate homographs. *Brain and Cognition, 55*(2), 396–399.
Salmelin, R. (2007). Clinical neurophysiology of language: The MEG approach. *Clinical Neurophysiology, 118*(2), 237–254.
Talairach, J., & Tournoux, P. (1988). *Co-planar stereotaxic atlas of the human brain.* New York: Thieme.
Tse, C. Y., Lee, C. L., Sullivan, J., Garnsey, S. M., Dell, G. S., Fabiani, M., et al. (2007). Imaging cortical dynamics of language processing with the event-related optical signal. *Proceedings of the National Academy of Sciences of the United States of America, 104*(43), 17157–17162.
Van Petten, C., & Luka, B. J. (2006). Neural localization of semantic context effects in electromagnetic and hemodynamic studies. *Brain and Language, 97*(3), 279–293.
Vandenberghe, R., Nobre, A. C., & Price, C. J. (2002). The response of left temporal cortex to sentences. *Journal of Cognitive Neuroscience, 14*(4), 550–560.
Vartiainen, J., Liljestrom, M., Koskinen, M., Renvall, H., & Salmelin, R. (2011). Functional magnetic resonance imaging blood oxygenation level-dependent signal and magnetoencephalography evoked responses yield different neural functionality in reading. *Journal of Neuroscience, 31*(3), 1048–1058.
Vigneau, M., Beaucousin, V., Herve, P. Y., Duffau, H., Crivello, F., Houde, O., et al. (2006). Meta-analyzing left hemisphere language areas: Phonology, semantics, and sentence processing. *NeuroImage, 30*(4), 1414–1432.
Xiang, H., Fonteijn, H., Norris, D., & Hagoort, P. (2010). Topographical functional connectivity pattern in the perisylvian language networks. *Cerebral Cortex, 20*(3), 549.
Zhu, Z., Hagoort, P., Zhang, J. X., Feng, G., Chen, H. C., Bastiaansen, M., et al. (2012). The anterior left inferior frontal gyrus contributes to semantic unification. *NeuroImage, 60*(4), 2230–2237.
Zhu, Z., Zhang, J. X., Wang, S., Xiao, Z., Huang, J., & Chen, H.-C. (2009). Involvement of left inferior frontal gyrus in sentence-level semantic integration. *NeuroImage, 47*(2), 756–763.